GEOPHYSICS, VOL. 63, NO. 3 (MAY-JUNE 1998); P. 948–956, 10 FIGS., 2 TABLES.

Framework for AVO gradient and intercept interpretation

John P. Castagna*, Herbert W. Swan‡, and Douglas J. Foster**

ABSTRACT

Amplitude variation with offset (AVO) interpretation may be facilitated by crossplotting the AVO intercept (A) and gradient (B). Under a variety of reasonable petrophysical assumptions, brine-saturated sandstones and shales follow a well-defined "background" trend in the A–B plane. Generally, A and B are negatively correlated for "background" rocks, but they may be positively correlated at very high V_P/V_S ratios, such as may occur in very soft shallow sediments. Thus, even fully brine-saturated shallow events with large reflection coefficients may exhibit large increases in AVO.

Deviations from the background trend may be indicative of hydrocarbons or lithologies with anomalous elastic properties. However, in contrast to the common assumptions that gas-sand amplitude increases with offset, or that the reflection coefficient becomes more negative with increasing offset, gas sands may exhibit a variety of AVO behaviors. A classification of gas sands based on location in the A–B plane, rather than on normal-incidence reflection coefficient, is proposed. According to this classification, bright-spot gas sands fall in quadrant III and have negative AVO intercept and gradient. These sands exhibit the amplitude increase versus offset which has commonly been used as a gas indicator. High-impedance gas sands fall in quadrant IV and have positive AVO intercept and negative gradient. Consequently, these sands initially exhibit decreasing AVO and may reverse polarity. These behaviors have been previously reported and are addressed adequately by existing classification schemes. However, quadrant II gas sands have negative intercept and positive gradient. Certain "classical" bright spots fall in quadrant II and exhibit decreasing AVO. Examples show that this may occur when the gas-sand shear-wave velocity is lower than that of the overlying formation. Common AVO analysis methods such as partial stacks and product ($A \times B$) indicators are complicated by this nonuniform gas-sand behavior and require prior knowledge of the expected gas-sand AVO response. However, Smith and Gidlow's (1987) fluid factor, and related indicators, will theoretically work for gas sands in any quadrant of the A–B plane.

INTRODUCTION

Amplitude variation with offset (AVO) analysis for nonbright-spot reservoirs is, in certain instances, facilitated by crossplotting extracted seismic parameters (Smith and Gidlow, 1987; Hilterman, 1987). As pointed out by Smith and Gidlow (1987) and others, the seismically extracted AVO intercept (A) and gradient (B) terms, in the absence of hydrocarbon-bearing strata, often form a well-defined "background trend" when crossplotted. The deviation from this background trend can be a hydrocarbon indicator.

Interpretation of such A versus B crossplots is complicated by (1) a lack of intuitive "feel" on the part of the interpreter for the physical significance of the B term, (2) the confounding effects of the seismic wavelet, (3) scatter caused by poor seismic data quality, and (4) nonpetrophysical influences on the extracted seismic parameters A and B. The purpose of this paper is to address item (1) by providing simple formulas and "rules of thumb" that aid AVO crossplot interpretation.

One approach to facilitate interpretation is to keep the A term (which is taken to be the normal-incidence P-wave reflection coefficient, R_P, and consequently is readily interpretable in physical terms) for one axis of the crossplot, but to recombine A and B to provide a second axis more directly related to rock properties. Hilterman (1987) and Verm and Hilterman (1995) use the change in Poisson's ratio across the interface ($\Delta\sigma$) for the second axis, whereas Castagna (1991) and (1993) uses the shear-wave reflection coefficient (R_S). Both these approaches use the Wiggins et al. (1983) approximation, and assume that

Manuscript received by the Editor August 26, 1996; revised manuscript received October 10, 1997.
*University of Oklahoma, SEC-810, School of Geology and Geophysics, 100 E. Boyd St., Norman, OK 73019-0628. E-mail: castagna@ou.edu.
‡ARCO Exploration and Production Technology, a division of Atlantic Richfield Co., 700 G Street, Rm 1340, Anchorage, AK 99501. E-mail: lanhws@expl.aai.arco.com.
**Formerly ARCO Exploration and Production Technology, currently Mobil Exploration and Production Technology Center, P.O. Box 650232, Dallas, TX 75265.

the compressional to shear-wave velocity ratio (V_P/V_S) is 2, or at least known (see Spratt et al. 1993). The penalty for this parameterization, of course, is that the quantities to be interpreted can no longer be readily related to the observed CDP gather by physical inspection.

A second approach, which avoids this difficulty, is to interpret the A versus B crossplot directly with the help of reference points such as the "fluid angle" of Foster et al. (1993) and the "fluid line" of Foster et al. (1997). With some reasonable petrophysical assumptions, we will show that equations for the "background trend" or "fluid line" can be derived, and that the resulting relationships are simple and easy to apply. Combined with rules of Koefoed (1955), these equations provide a simple framework for the interpretation of AVO crossplots.

ANGULAR REFLECTION COEFFICIENTS

Let us consider two semi-infinite isotropic homogeneous elastic half-spaces in contact at a plane interface. For an incident plane wave, the reflection coefficient variation with angle of incidence is given by the well-known Knott-Zoeppritz equations. These equations are unwieldy and defy direct physical insight. Fortunately, for small variations in layer parameters and angles of incidence commonly encountered in seismic reflection applications, these equations can be accurately approximated (e.g., Bortfeld, 1961; Richards and Frasier, 1976; Aki and Richards, 1980; Shuey, 1985). Following Swan (1993), we express the Aki and Richards (1980) form of the Richards and Frasier (1976) approximation in terms of the angular reflection coefficients A, B, and C:

$$R(\theta) \approx A + B\sin^2(\theta) + C\sin^2(\theta)\tan^2(\theta) \qquad (1)$$

where R is the reflection coefficient as a function of the average angle θ (taken as a further approximation to be the angle of incidence) with

$$A = \frac{1}{2}\left(\frac{\Delta V_P}{\langle V_P\rangle} + \frac{\Delta\rho}{\langle\rho\rangle}\right); \qquad (2)$$

$$B = \frac{1}{2}\frac{\Delta V_P}{\langle V_P\rangle} - 2\left(\frac{\langle V_S\rangle}{\langle V_P\rangle}\right)^2\left(2\frac{\Delta V_S}{\langle V_S\rangle} + \frac{\Delta\rho}{\langle\rho\rangle}\right); \qquad (3)$$

$$C = \frac{1}{2}\frac{\Delta V_P}{\langle V_P\rangle}, \qquad (4)$$

where ΔV_P is the change in compressional velocity across the interface ($V_{P2} - V_{P1}$), $\langle V_P\rangle$ is the average compressional velocity across the interface $[(V_{P2} + V_{P1})/2]$, $\Delta\rho$ is the change in density across the interface ($\rho_2 - \rho_1$), $\langle\rho\rangle$ is the average density across the interface $[(\rho_2 + \rho_1)/2]$, ΔV_S is the change in shear velocity across the interface ($V_{S2} - V_{S1}$), and $\langle V_S\rangle$ is the average shear velocity across the interface $[(V_{S2} + V_{S1})/2]$, with V_{P1}, V_{S1}, ρ_1 and V_{P2}, V_{S2}, ρ_2 being the medium properties in the first (overlying) and second (underlying) media, respectively. Note that A is the linearized form of the normal-incidence compressional-wave reflection coefficient (R_P).

RELATIONSHIPS BETWEEN A AND B

The parameters V_P, V_S, and ρ are often highly correlated, with deviations attributable to hydrocarbons or unusual lithologies. These correlations imply relationships between the angular reflection coefficients A and B.

Gardner's equation

We assume that the "background" consists of brine-saturated sandstones and shales and, to first order, that density is a constant factor times the velocity raised to some arbitrary power g. Gardner et al. (1974) showed that g is about equal to 1/4 for most sedimentary rocks. For small changes in velocity, we have

$$\frac{\Delta\rho}{\langle\rho\rangle} \sim g\frac{\Delta V_P}{\langle V_P\rangle}. \qquad (5)$$

This relationship can be violated strongly at lithologic boundaries, however. The significance of such deviations is discussed below.

V_S versus V_P relationships

Within a sequence of fully brine-saturated rocks of similar age and composition, we can often assume, to a first order, a linear relationship between V_P and V_S without lithologic differentiation. For example, Castagna et al. (1985) showed that brine-saturated sandstones and shales often roughly follow a given trend, referred to as the "mudrock" line. (Because variance about this trend depends on local geology, we cannot offer a "global" variance number; however, deviations on the order of 5% are common. Such deviations can significantly effect AVO analysis.) Rather than restrict ourselves to the particular coefficients of the mudrock line, let us assume simply that, for a particular depth window at a given locality, there is some linear relationship between V_P and V_S:

$$V_P = mV_S + c, \qquad (6)$$

where m and c are empirical coefficients.

General intercept versus gradient equation

Combining equations (2) through (6) yields a general equation for "background" reflections in the A–B plane:

$$B = \frac{A}{1+g}\left[1 - 4\frac{\langle V_S\rangle}{\langle V_P\rangle}\left(\frac{2}{m} + g\frac{\langle V_S\rangle}{\langle V_P\rangle}\right)\right]. \qquad (7)$$

This general relationship allows for arbitrary perturbations of the Gardner and V_P versus V_S trend curves. We now consider four special cases for the background trend.

The background trend: Constant V_P/V_S and constant density

If V_P/V_S is constant, c must vanish, and

$$m = V_P/V_S = \langle V_P\rangle/\langle V_S\rangle = \Delta V_P/\Delta V_S. \qquad (8)$$

Setting $\Delta\rho = 0$ (for constant density) in equation (2) while substituting $g = 0$ and equation (8) into equation (7) yields

$$A = \tfrac{1}{2}\Delta V_P/\langle V_P\rangle \qquad (9)$$

and

$$B = \left[1 - 8\left(\frac{\langle V_S\rangle}{\langle V_P\rangle}\right)^2\right]A. \qquad (10)$$

Equation (10) is equivalent to equation (14) in Foster et al. (1997).

The background trend: Constant V_P/V_S and Gardner density

Instead of assuming constant density, we now honor Gardner's relation (5). Setting $g = 1/4$ and $m = \langle V_P\rangle/\langle V_S\rangle$ (constant V_P/V_S) yields

$$A = \tfrac{5}{8}\Delta V_P/\langle V_P\rangle \tag{11}$$

and

$$B = \frac{4}{5}\left[1 - 9\left(\frac{\langle V_S\rangle}{\langle V_P\rangle}\right)^2\right]A. \tag{12}$$

Equation (12) indicates that lines of constant $\langle V_P\rangle/\langle V_S\rangle$ should pass through the origin. Furthermore, the slope of the predicted "background trend" depends only on the background $\langle V_P\rangle/\langle V_S\rangle$ ratio. Figure 1 shows that as $\langle V_P\rangle/\langle V_S\rangle$ increases, the slope of the background trend becomes more positive (the trend rotates counterclockwise for A plotted along the x-axis).

It is useful to note that for the Wiggins approximation ($\langle V_P\rangle/\langle V_S\rangle = 2.0$), from equations (3) and (4) we have $B = -A$ irrespective of density and velocity relationships. Thus, scatter introduced by violation of the Gardner equation should be small when the background $\langle V_P\rangle/\langle V_S\rangle$ is about 2.

Since

$$R_P - R_S \sim \frac{1}{2}\left(\frac{\Delta V_P}{\langle V_P\rangle} - \frac{\Delta V_S}{\langle V_S\rangle}\right), \tag{13}$$

where R_S is the normal-incidence shear-wave reflection coefficient, it is evident that $R_P - R_S$ is always about zero for constant $\langle V_P\rangle/\langle V_S\rangle$. Furthermore, for the particular case when $\langle V_P\rangle/\langle V_S\rangle = 2.0$, we have

$$R_P - R_S \sim (A + B)/2 = 0. \tag{14}$$

Also note in equation (12) that $B = 0$ when $\langle V_P\rangle/\langle V_S\rangle = 3$.

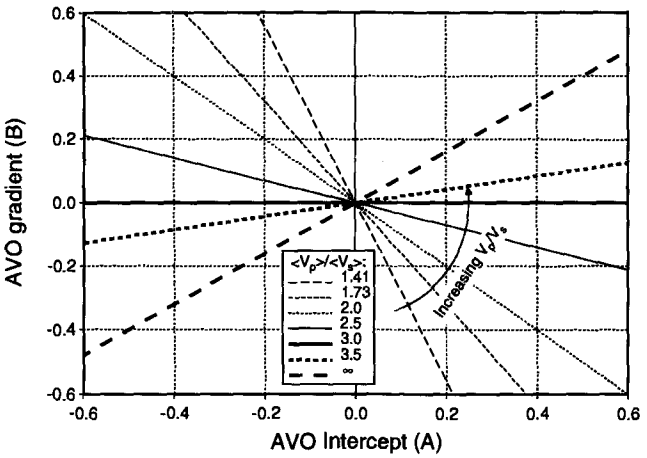

FIG. 1. Zero-offset reflection coefficient (A) versus the AVO gradient (B) assuming constant V_P/V_S and Gardner's relation. The background trend rotates counterclockwise as V_P/V_S increases.

The background trend: Linear V_P versus V_S

Although constant $\langle V_P\rangle/\langle V_S\rangle$ may be a useful assumption for limited depth ranges, a more general assumption is a linear relationship between V_P and V_S. From equation (6), we have directly

$$\langle V_P\rangle = m\langle V_S\rangle + c; \tag{15}$$

$$\frac{\Delta V_P}{\Delta V_S} = m = \frac{\langle V_P\rangle}{\langle V_S\rangle}\left(\frac{\langle V_P\rangle - c}{\langle V_P\rangle}\right); \tag{16}$$

$$\frac{\Delta V_S}{\langle V_S\rangle} = \frac{\Delta V_P}{\langle V_P\rangle}\left(\frac{\langle V_P\rangle}{\langle V_P\rangle - c}\right), \tag{17}$$

and

$$R_P - R_S \sim -\frac{1}{2}\frac{\Delta V_P}{\langle V_P\rangle}\left(\frac{c}{\langle V_P\rangle - c}\right). \tag{18}$$

From equation (18), we can view $R_P - R_S$ as the P-wave velocity contrast scaled by a slowly varying background term. $R_P - R_S$ will be magnified as the background velocity approaches the constant c from above and diminished at high background velocities. Similarly, the "pseudo-Poisson's ratio reflectivity," as defined by Smith and Gidlow (1987) and popularized by Verm and Hilterman (1995) among others is given by

$$\frac{\Delta\sigma}{\langle\sigma\rangle} \sim 2(R_P - R_S), \tag{19}$$

where $\Delta\sigma$ is the change in Poisson's ratio across the interface and $\langle\sigma\rangle$ is the average Poisson's ratio.

Substituting $g = 1/4$ and

$$\frac{\langle V_S\rangle}{\langle V_P\rangle} = \frac{1}{m}\left(1 - \frac{c}{\langle V_P\rangle}\right) \tag{20}$$

into equation (7) yields

$$B = \frac{4}{5}\left[1 - \frac{1}{(m\langle V_P\rangle)^2}(\langle V_P\rangle - c)(9\langle V_P\rangle - c)\right]A, \tag{21}$$

with A given by equation (11).

According to equation (21):

1) The background trend passes through the origin ($A = B = 0$).
2) As shown in Figure 2, as $\langle V_P\rangle$ decreases [and $\langle V_P\rangle/\langle V_S\rangle$ increases according to equation (15)], the background trend slope becomes more positive (rotates counterclockwise). This figure assumes the shale mudrock trend slope m of 1.16 and an intercept c of 1.36 km/s given in Castagna et al. (1985). Note that the background trend slope changes dramatically for velocities lower than 2.5 km/s. One might expect greater difficulty in establishing a well-defined background trend at these lower velocities.
3) These conclusions are similar to those for a constant $\langle V_P\rangle/\langle V_S\rangle$ ratio. However, for a given $\langle V_P\rangle/\langle V_S\rangle$, the slopes are not necessarily equivalent for the two cases. Keep in mind, that for a linear V_P–V_S relationship, V_P/V_S varies across the interface rather than remaining constant. This results in a different background trend at a given $\langle V_P\rangle/\langle V_S\rangle$.

4) Equation (21) reduces to equation (12) when c is zero.

Assuming constant density ($g=0$), rather than Gardner's relation, gives

$$B=\left[1-\frac{8}{m}\frac{\langle V_S\rangle}{\langle V_P\rangle}\right]A=\left[1-8\left(\frac{\langle V_S\rangle}{\langle V_P\rangle}\right)^2\frac{\langle V_P\rangle}{\langle V_P\rangle-c}\right]A, \tag{22}$$

which is equivalent to equation (15) of Foster et al. (1997).

Background trend comparison

Figure 3 shows the calculated slope of the background trend (B/A) as a function of $\langle V_P\rangle/\langle V_S\rangle$ for

1) Constant density and constant V_P/V_S from equation (10)
2) Gardner density and constant V_P/V_S from equation (12)

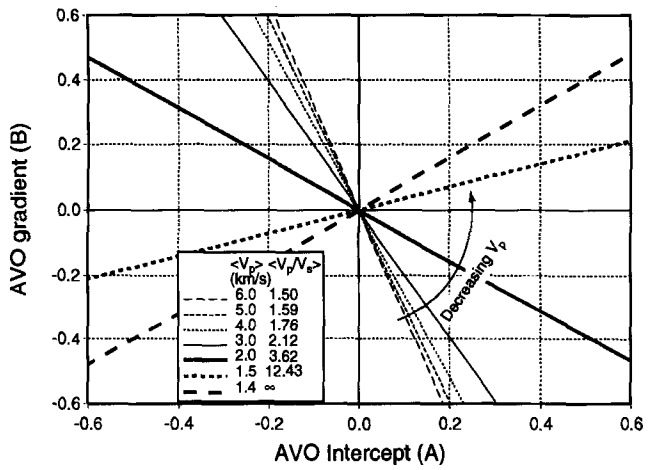

FIG. 2. Zero-offset reflection coefficient (A) versus the AVO gradient (B) assuming a linear V_P versus V_S trend ($m=1.16, c=1.36$ km/s) and Gardner's relation. The background trend rotates counterclockwise as V_P decreases.

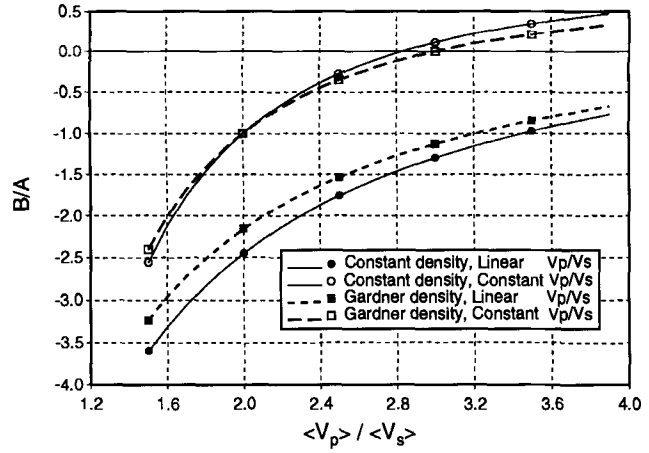

FIG. 3. B/A versus $\langle V_P\rangle/\langle V_S\rangle$ for various background trend assumptions: constant V_P/V_S and constant density, constant V_P/V_S and Gardner density, mudrock V_P versus V_S and constant density, mudrock V_P versus V_S and Gardner density. In all cases, B/A increases with increasing background $\langle V_P\rangle/\langle V_S\rangle$.

3) Constant density and linear V_P versus V_S computed for the mudrock trend ($m=1.16$ and $c=1.36$ km/s), using equation (7)
4) Gardner density ($g=1/4$) and linear (mudrock) V_P versus V_S from equation (7).

For the small elastic contrasts implicit in the Aki and Richards (1980) approximations, a linear relationship exists between the background B and A. [Foster et al. (1997) show how this linear relationship is violated for large elastic contrasts, but only if $\langle V_P\rangle/\langle V_S\rangle \neq 2$.] B/A increases with increasing background $\langle V_P\rangle/\langle V_S\rangle$ for all cases. It is important to note that the density relationship is less important than the V_P versus V_S relationship. The constant V_P/V_S and linear V_P versus V_S assumptions give distinctly different background trends. For the constant V_P/V_S cases, B/A becomes positive at V_P/V_S ratios of about 3 and higher. Thus, a large negative A can result in a large negative B leading to an amplitude magnitude increase with offset for nonpay background rocks. This could occur in very unconsolidated sands and shales where V_P and V_S are not as well correlated as in well consolidated rocks. See the comparison of Hamilton's (1979) data to the mudrock trend in Castagna et al. (1985). For the linear V_P versus V_S relationship, B/A becomes positive only at very high $\langle V_P\rangle/\langle V_S\rangle$ ratios approaching 10.

DEVIATIONS FROM PETROPHYSICAL RELATIONSHIPS

Imperfect adherence to the assumed background petrophysical relationships introduces scatter about the background trend on an A versus B crossplot. A key issue for AVO interpretation is the magnitude of this variation relative to deviations caused by hydrocarbons. Smith and Gidlow (1987) provide an example where violation of the Gardner density assumption is a second-order effect on the observed seismic data. In our experience, for binary sandstone/shale intervals, scatter due to nonpetrophysical factors (i.e., anything that causes seismic amplitudes to differ from reflection coefficients) is often larger than scatter introduced by imperfect adherence to Gardner density and linear V_P versus V_S assumptions. As noted above, scatter due to violation of the density assumption is minimal at $\langle V_P\rangle/\langle V_S\rangle$ ratios close to 2. For a given P-wave velocity, salt exhibits unusually low density (Gardner et al., 1974) and, therefore, may deviate significantly from the background trend. Petrophysical trend curves for various lithologies are given in Castagna et al. (1993).

Of course, the most interesting deviation from background petrophysical relationships results from replacement of brine in the pore space by hydrocarbons, particularly gas, for which the effects are most pronounced. Assuming no associated geological or chemical effects, the mechanical replacement of gas for brine using Gassmann's equations reduces $\langle V_P\rangle/\langle V_S\rangle$ and causes ΔV_P and $\Delta\rho$ to become more negative. Thus, by equations (2) and (3), for a top-of-sand reflection, partial gas saturation causes both A and B to become more negative than for the corresponding fully brine-saturated sand. This is illustrated in Figure 4, which shows calculated AVO intercepts and gradients for pairs of shale/gas sand and shale/brine sand reflectors. The shale over brine-sand reflection coefficients vary from strongly positive to strongly negative, but were selected to have the same average P-wave velocity. Intercepts and gradients were then calculated using Gardner's relation and the mudrock trend, and were found to lie along the straight line predicted by

equation (15). Gassmann's equations were then used to substitute gas for brine in the sands. The reflection coefficients for the corresponding gas sands also fall along a straight line to the lower left of the background trend. Each tie line moves toward more negative A and B from brine sand to gas sand.

Figure 5 shows brine sand–gas sand tie lines for 25 sets of primarily in situ sonic-log measurements in brine sands, gas sands, and shales reported in Castagna and Smith (1994). As noted in that paper, most of the shear-wave velocities were measured directly with dipole or full-waveform sonic logs, or measured in the laboratory. Although the validity of sonic log readings in gas sands is questionable, the gas sands do tend to plot to the lower left of the brine sands. In addition to experimental error, geological variation such as porosity differences between the brine sands and corresponding gas sands will cause deviations from predictions made using Gassmann's equations. Note also that the background velocity is different for each brine sand, so one should not expect all of the datapoints to fall along a single background trend. Nevertheless, the overall tendency of the gas sands to deviate from the brine sands is clear. This is the basis for Smith and Gidlow's (1987) hydrocarbon detection methodology using the fluid factor (ΔF), which is a measure of the deviation from the background trend:

$$\Delta F = \frac{\Delta V_P}{\langle V_P \rangle} - m\frac{\langle V_S \rangle}{\langle V_P \rangle}\frac{\Delta V_S}{\langle V_S \rangle}. \tag{23}$$

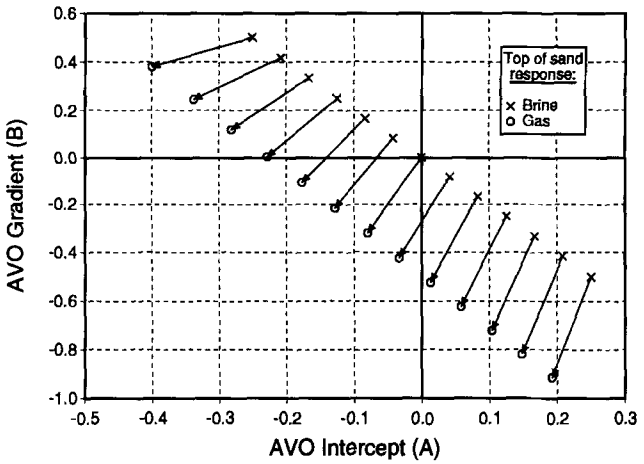

FIG. 4. Brine sand–gas sand tie lines for shale over brine-sand reflections having an average P-wave velocity of 3 km/s and which conform to Gardner and mudrock petrophysical trend curves ($g = 0.25, m = 1.16, c = 1.36$ km/s) and Gassmann's equations.

KOEFOED'S RULES AND GAS SAND CLASSIFICATIONS

Koefoed (1955) manually calculated reflection coefficient versus offset using the exact Zoeppritz equations for about twenty different models. His observations of the systematics of reflection coefficient variation are known as Koefoed's rules. Shuey (1985) showed that these rules are readily discerned from the Richards and Frasier (1976) approximation. Here, we discuss two of these rules, as broadened by Shuey (1985), in the context of an A versus B crossplot (Figure 6). Consider a plane interface between two infinite half-spaces:

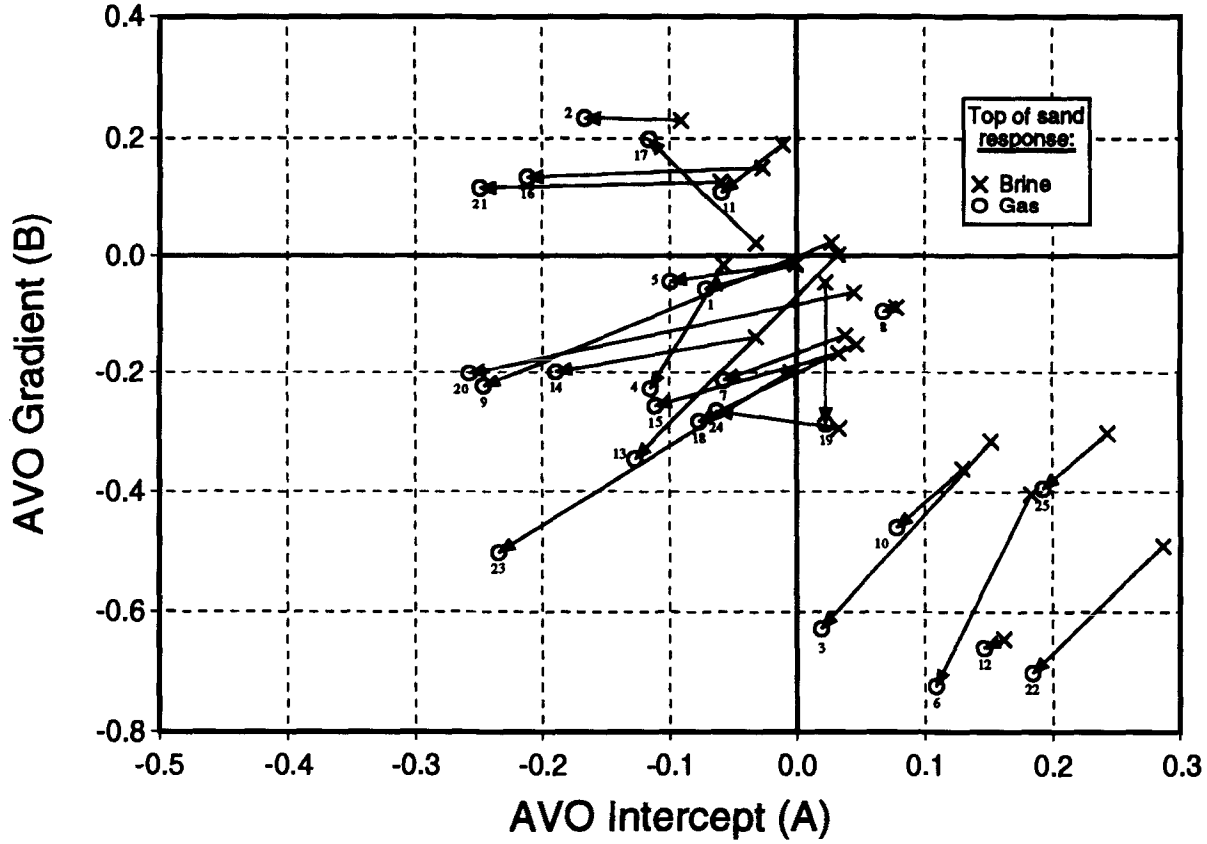

FIG. 5. The movement of AVO reflection coefficients as gas replaces brine within a sandy layer below shale for 25 sets of shale, brine-sand, and gas-sand velocities and densities reported in Castagna and Smith (1994).

Rule 1.—"... an increase of Poisson's ratio for the underlying medium causes an increase of the reflection coefficient at the larger angles of incidence."

Rule 2.—"When ... Poisson's ratio for the incident medium is increased, the reflection coefficient at the larger angles of incidence is thereby decreased."

Although not stated explicitly by Koefoed (1955), these rules also suggest that a decrease in Poisson's ratio for the lower medium causes a decrease in reflection coefficient at larger angles of incidence. This is the case for a classical top of gas-sand reflector as originally described by Ostrander (1984). One should keep in mind that by "decrease at larger angles of incidence," Koefoed should be interpreted as saying "become more negative at larger angles of incidence relative to the prior state." In other words, B is made more negative by adding hydrocarbons (thereby decreasing Poisson's ratio) in the underlying medium. A is also made more negative by the addition of hydrocarbons. The effect of adding hydrocarbons to a layer otherwise falling on the background trend of Figure 6 is for the top of the unit to plot below the background trend (more negative A and B). Conversely, the bottom of a gas sand should plot above the background trend (more positive A and B), assuming the medium immediately underlying the gas sand has properties similar to the properties of the medium overlying the gas sand. Top of gas-sand amplitude increases with offset only for gas sands whose tops plot in the third quadrant of Figure 6. Here, A and B are negative and amplitude becomes more negative (and greater in magnitude) with increasing offset.

The class I, II and III curves of Figure 7 show the Rutherford and Williams (1989) classification for gas sands. Note that this classification is based only on the normal-incidence reflection coefficient ($R_P = A$). Class I sands are high impedance relative to the overlying shales. Class II sands have low normal-incidence reflectivity (small impedance contrast). Class III sands are lower impedance than the overlying shales (classical bright spots), and exhibit increasing reflection magnitude with offset. The importance of this classification has been in demonstrating that reflection coefficients need not increase with offset for gas sands as was commonly assumed previously. In particular, for high-impedance gas sands, reflection coefficients decrease with increasing offset. Unfortunately, one could conclude from the first three curves that gas-sand reflection coefficients always become more negative with increasing offset for all three classes. In fact, a fourth class of sand (class IV) exists for which the introduction of gas causes its reflection coefficient to become more positive with increasing offset, yet decrease in magnitude with increasing offset.

This augmented Rutherford and Williams (1989) classification for gas sands is also superimposed on Figure 6. Consider class III gas sands falling in quadrant III of Figure 6. They have negative A and B, and reflection magnitude increases versus offset. Class IV gas sands, which fall in quadrant II, also have a large negative A but positive B. These are true bright spots, but reflection magnitude decreases with increasing offset. This is illustrated in Figure 8 for a low-impedance brine sand which falls on the background trend. Although the reflection coefficients are large, the Shuey (1985) two-term approximation is good to about 30° local angle of incidence. For angles less than this, B is positive for both brine and gas sands, and magnitude decreases with increasing offset in both cases. Since the AVO gradient from a class IV brine sand may be almost identical

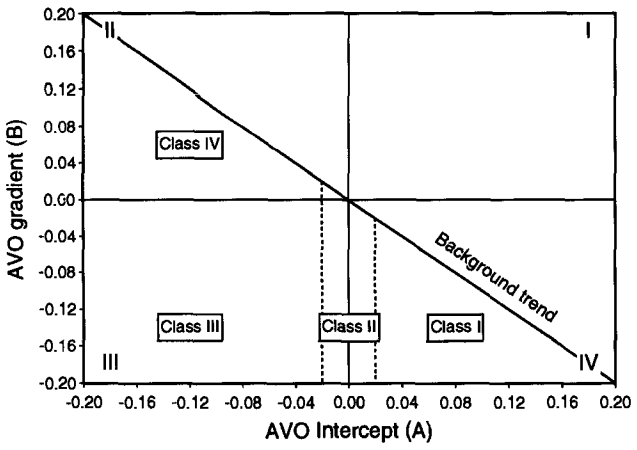

FIG. 6. AVO intercept (A) versus gradient (B) crossplot showing four possible quadrants. For a limited time window, brine-saturated sandstones and shales tend to fall along a well-defined background trend. Top of gas-sand reflections tend to fall below the background trend, whereas bottom of gas-sand reflections tend to fall above the trend. Augmented Rutherford and Williams (1989) gas sand classes are also indicated for reference.

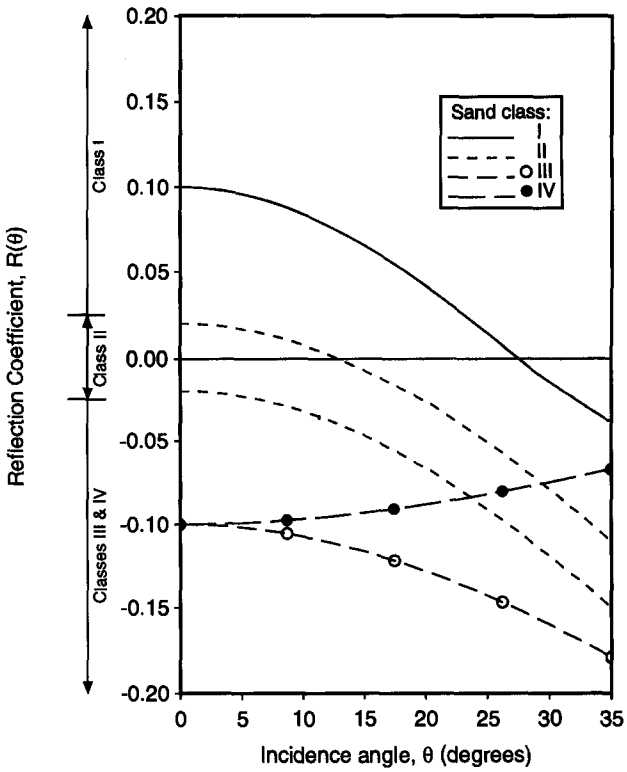

FIG. 7. Plane-wave reflection coefficients at the top of each Rutherford and Williams (1989) classification of gas sand. Class IV sands, not discussed by Rutherford and Williams, have a negative normal-incidence reflection coefficient, but decrease in amplitude magnitude with offset.

to the gradient from a class IV gas sand (see Figures 5 and 8), these gas sands may be difficult to detect by comparing partial offset stacks.

Table 1 summarizes the possible AVO behavior for the various types of gas sand. We find either an A–B quadrant identification or an augmented Rutherford and Williams classification to be more informative than one based only on the normal-incidence compressional-wave reflection coefficient.

EXAMPLE: LOW-IMPEDANCE GAS SAND OVERLAIN BY HIGH-VELOCITY UNIT

Class IV gas sands frequently occur when a porous sand is overlain by a high-velocity unit, such as a hard shale (e.g., siliceous or calcareous), siltstone, tightly cemented sand, or a carbonate. Table 2 gives well log V_P, V_S, and density for a gas sand and an overlying shale and tight unit (courtesy of Jeremy Greene, ARCO International Oil and Gas Co.) As shown in Figure 9, when the gas sand is overlain by shale, the AVO intercept (A) is large and negative and the AVO gradient (B) is negative. This falls in quadrant III of Figure 6 and represents a typical well-behaved Rutherford and Williams (1989) class III gas sand. However, when the overlying unit is a tight unit (Figure 10), the AVO intercept (A) is large and negative, but the AVO gradient (B) is positive. Thus, although one would classify this reflection as class III based on compressional-wave impedance contrast alone, the reflector falls in quadrant II of Figure 6, since its amplitude decreases with offset. Furthermore, the same gas sand produces very different AVO behavior depending on its overlying shale. Thus, it is incorrect to classify a reflector based on the properties of the sand alone.

To understand this unusual but highly significant behavior, we refer to the original Richards and Frasier (1976) approximation as given in Aki and Richards (1980):

$$R(\theta) = \frac{1}{2}\left(1 - 4\langle V_S\rangle^2 p^2\right)\frac{\Delta\rho}{\langle\rho\rangle} + \frac{1}{2\cos^2\theta}\frac{\Delta V_P}{\langle V_P\rangle} - 4\langle V_S\rangle^2 p^2 \frac{\Delta V_S}{\langle V_S\rangle}, \quad (24)$$

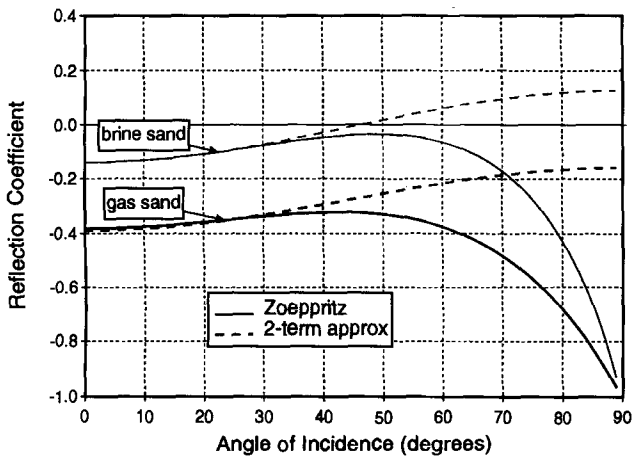

FIG. 8. Plane-wave reflection coefficient versus angle of incidence for the top of a class IV (quadrant II) gas sand, and the corresponding brine-sand reflection. The model parameters are: shale—$V_P = 3.24$ km/s, $V_S = 1.62$ km/s, $\rho = 2.34$ gm/cm^3; brine sand—$V_P = 2.59$ km/s, $V_S = 1.06$ km/s, $\rho = 2.21$ gm/cm^3; gas sand—$V_P = 1.65$ km/s, $V_S = 1.09$ km/s, $\rho = 2.07$ gm/cm^3. The solid lines are the full Zoeppritz solution. The dashed lines are the two-term Shuey (1985) approximation.

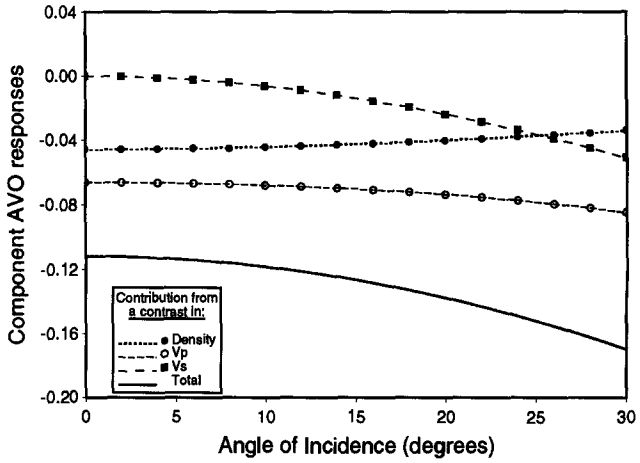

FIG. 9. Richards and Frasier (1976) decomposition for a class III (quadrant III) shale over gas-sand reflection showing the AVO contribution from fractional changes in density ρ, compressional velocity V_P, and shear velocity V_S.

Table 2. Well log velocities and densities for an East African gas sand and overlying strata (provided by Jeremy Greene).

Lithology	V_P (m/s)	V_S (m/s)	ρ (gm/cm^3)
Shale	2900	1330	2.29
Tight unit	3250	1780	2.44
Gas sand	2540	1620	2.09

Table 1. Top gas sand reflection coefficient versus offset behavior for the three Rutherford and Williams (1989) classes I–III assuming a typical "background" trend with negative slope. Class IV sands, though not explicitly discussed by Rutherford and Williams, may be considered to be a subdivision of their class III sands.

Class	Relative impedance	Quadrant	A	B	Remarks
I	Higher than overlying unit	IV	+	−	Reflection coefficient (and magnitude) decrease with increasing offset
II	About the same as the overlying unit	III or IV	±	−	Reflection magnitude may increase or decrease with offset, and may reverse polarity
III	Lower than overlying unit	III	−	−	Reflection magnitude increases with offset
IV	Lower than overlying unit	II	−	+	Reflection magnitude decreases with offset

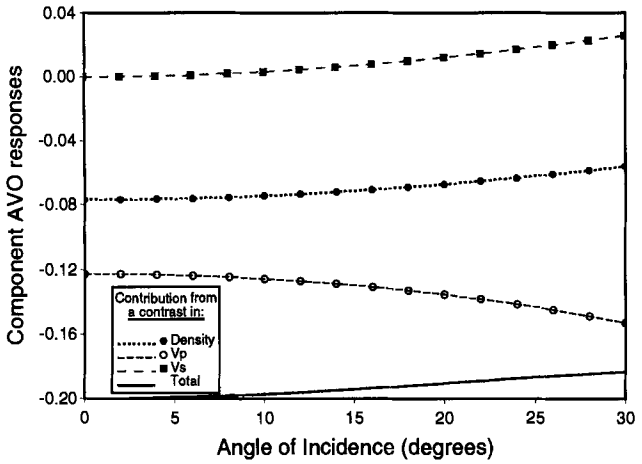

FIG. 10. Richards and Frasier (1976) decomposition for the same gas sand as in Figure 9, but now overlain with a calcareous tight unit. Its total AVO response is now class IV (quadrant II), due to the reversal of its shear velocity component.

where p is the ray parameter ($\sin\theta/V_P$) and θ is the average of the angle of incidence and refraction.

Equation (24) can be used to approximately decompose the contributions to the reflection coefficient variation with offset by changes in V_P, V_S, and density (ρ). As shown in Figures 9 and 10, the contribution due to the density contrast has a positive slope in both cases, whereas the contribution due to the V_P contrast has a negative slope. However, the key parameter is the shear-wave velocity contrast. Note that at zero offset, the shear contrast contributes nothing to the reflection coefficient. However, when ΔV_S is positive (as is the case for the shale over gas sand example; Figure 9), the shear contribution becomes more negative with increasing offset, thereby enhancing the total amplitude increase with offset. On the other hand, when ΔV_S is negative (tight unit over gas sand; Figure 10), the shear contribution becomes more positive with increasing offset. The net result is a small decrease in the total reflection coefficient with increasing offset, thereby resulting in a class IV sand in quadrant II, having a positive B.

Based on equation (24), we can generalize for class III and IV gas sands that an increase in shear-wave velocity across the top sand interface enhances the amplitude increase with offset, whereas a decrease in shear-wave velocity diminishes the amplitude increase with offset and may result in an amplitude decrease with offset. It is important to note that whereas class IV gas sands exhibit unexpected absolute AVO behavior according to established rules of thumb and are difficult to interpret on partial offset stacks or using product ($A \times B$) indicators, they do not confound A versus B crossplot based indicators such as Smith and Gidlow's (1987) fluid factor.

CONCLUSIONS AND DISCUSSION

Reasonable petrophysical assumptions for sandstone-shale intervals result in linear background trends for limited depth ranges on AVO intercept (A) versus gradient (B) crossplots. In general, the background trend B/A becomes more positive with increasing background $\langle V_P\rangle/\langle V_S\rangle$. Thus, if too large a depth range is selected for A versus B crossplotting, and background $\langle V_P\rangle/\langle V_S\rangle$ varies significantly (as would be caused by compaction), a variety of background trends may be superimposed. This would result in a less well-defined background relationship. For very high $\langle V_P\rangle/\langle V_S\rangle$, as would occur in very soft, shallow, brine-saturated sediments, the background trend B/A becomes positive, and nonhydrocarbon-related reflections may exhibit increasing AVO and show false positive anomalies on $A \times B$ product displays or improperly calibrated fluid-factor sections.

Deviations from the background trend may be indicative of hydrocarbons. This is the basis for Smith and Gidlow's (1987) fluid factor and related indicators. Inspection of the A–B plane reveals that gas sands may exhibit variable AVO behavior. We suggest that hydrocarbon bearing sands should be classified according to their location in the A–B plane, rather than by their normal-incidence reflection coefficient alone.

Class I gas sands have a positive normal-incidence reflection coefficient, lie in quadrant IV, and decrease in amplitude magnitude with increasing offset faster than the background trend. Class II gas sands have a small normal-incidence coefficient (less than 0.02 in magnitude), but achieve a greater amplitude magnitude than the background at sufficiently high offsets. Polarity reversals are common with this type of reflector, which can lie in either quadrants II, III, or IV. Class III gas sands have a strongly negative normal-incidence reflection coefficient, which becomes even more negative with increasing offset. These sands lie in quadrant III. Class IV gas sands also have a negative normal-incidence reflection coefficient, but lie in quadrant II and decrease in amplitude magnitude with offset. They do so more slowly than background reflections with the same intercept.

AVO product indicators (such as A times B) will show positive anomalies only for quadrant III gas sands. Interpretation of product indicators and partial stacks is difficult without prior knowledge of the expected gas-sand quadrant. Alternatively, the fluid factor and related indicators will theoretically work for any class of gas sand in any quadrant.

ACKNOWLEDGMENTS

This research was supported by ARCO Exploration and Production Technology, Mobil Exploration and Production Technology Center, and the Gas Research Institute under contract number 5090-212-2050. Special thanks are owed to Ken Tubman, Jeremy Greene, Tim Fasnacht, and Manik Talwani for their support.

REFERENCES

Aki, K., and Richards, P. G., 1980, Quantitative seismology: Theory and methods: W. H. Freeman and Co.

Bortfeld, R., 1961, Approximation to the reflection and transmission coefficients of plane longitudinal and transverse waves: Geophys. Prosp., **9**, 485–503.

Castagna, J. P., 1991, Seismic lithology overview: 61st Ann. Internat. Mtg., Soc. Expl. Geophys., Expanded Abstracts, 1051–1053.

———1993, AVO analysis—Tutorial and review, *in* Castagna, J. P., and Backus, M. M., Eds., Offset-dependent reflectivity—Theory and practice of AVO analysis: Soc. Expl. Geophys., 3–36.

Castagna, J. P., Batzle, M. L., and Eastwood, R. L., 1985, Relationships between compressional and shear-wave velocities in clastic silicate rocks: Geophysics, **50**, 551–570.

Castagna, J. P., Batzle, M. L., and Kan, T. K., 1993, Rock physics—The link between rock properties and AVO response, *in* Castagna, J. P., and Backus, M. M., Eds., Offset-dependent reflectivity—Theory and practice of AVO analysis: Soc. Expl. Geophys., 135–171.

Castagna, J. P., and Smith, S. W., 1994, Comparison of AVO indicators: A modeling study: Geophysics, **59**, 1849–1855.

Foster, D. J., Smith, S. W., Dey-Sarkar, S., and Swan, H. W., 1993, A

closer look at hydrocarbon indicators: 63rd Ann. Internat. Mtg., Soc. Expl. Geophys., Expanded Abstracts, 731–733.
Foster, D. J., Keys, R. G., and Schmitt, D. P., 1997, Detecting subsurface hydrocarbons with elastic wavefields, *in* Chavent, G., Papanicolaou, G., Sacks, P., and Symes, W., Eds., Inverse problems in wave propagation: Springer-Verlag.
Gardner, G. H. F., Gardner, L. W., and Gregory, A. R., 1974, Formation velocity and density—The diagnostic basis for stratigraphic traps: Geophysics, **39**, 770–780.
Hamilton, E. L., 1979, V_P/V_S and Poisson's ratios in marine sediments and rocks: J. Opt. Soc. Am., **66**, 109–1101.
Hilterman, F., 1987, Seismic lithology: Unpublished course notes: Soc. Expl. Geophys.
Koefoed, O., 1955, On the effect of Poisson's ratios of rock strata on the reflection coefficients of plane waves: Geophys. Prosp., **3**, 381–387.
Ostrander, W. J., 1984, Plane-wave reflection coefficients for gas sands at non-normal angles of incidence: Geophysics, **49**, 1637–1648.
Richards, P. G., and Frasier, C. W., 1976, Scattering of elastic wave from depth-dependent inhomogeneities: Geophysics, **41**, 441–458.
Rutherford, S. R., and Williams, R. H., 1989, Amplitude-versus-offset variations in gas sands: Geophysics, **54**, 680–688.
Shuey, R. T., 1985, A simplification of the Zoeppritz equations: Geophysics, **50**, 609–614.
Smith, G., and Gidlow, P. M., 1987, Weighted stacking for rock property estimation and detection of gas: Geophys. Prosp., **35**, 993–1014.
Spratt, R. S., Goins, N. R., and Fitch, T. J., 1993, Pseudo-shear—The analysis of AVO, *in* Castagna, J. P., and Backus, M. M., Eds., Offset-dependent Reflectivity—Theory and practice of AVO analysis: Soc. Expl. Geophys., 37–56.
Swan, H. W., 1993, Properties of direct AVO hydrocarbon indicators, *in* Castagna, J. P., and Backus, M. M., Eds., Offset-dependent Reflectivity—Theory and practice of AVO analysis: Soc. Expl. Geophys., 78–92.
Verm, R., and Hilterman, F., 1995, Lithology color-coded seismic sections: The calibration of AVO crossplotting to rock properties: The Leading Edge, **14**, No. 7, 847–853.
Wiggins, R., Kenny, G. S., S., G., and McClure, C. D., 1983, A method for determining and displaying the shear-velocity reflectivities of a geologic formation: European Patent Application 0113944.